

# Steady Operation of an FRC Thruster on Martian Atmosphere and Liquid Water Propellants

David Kirtley<sup>1</sup>, Anthony Pancotti<sup>2</sup>, John Slough<sup>3</sup>, and Chris Pihl

MSNW LLC, Redmond, WA 98052

## Nomenclature

$B_b, B_{bias}$	=	magnitude of preexisting (vacuum) axial magnetic field
$B_\omega$	=	amplitude of rf rotating magnetic field
$\Delta B_z$	=	axial magnetic field change due to RMF driven currents (superscript M denotes maximum)
$B_{ext}$	=	magnitude of magnetic field external (radially) to the FRC
$\beta$	=	plasma pressure normalized to external (vacuum) field
$C$	=	capacitance value
$\delta$	=	classical skin depth = $(2\eta/\mu_0\omega)^{1/2}$
$\mathbf{E}$	=	electric field vector (subscripts r, $\theta$ , z denote cylindrical components)
$e$	=	unit of electron charge
$E_k$	=	propellant kinetic energy
$E_{k\_RMF}$	=	kinetic energy derived from electromagnetic input
$E_{k\_th}$	=	kinetic energy derived from conversion of plasma thermal energy
$E_{ion}$	=	ionization energy
$E_\Omega$	=	energy input from Ohmic heating
$\varepsilon$	=	Hall scaling parameter
$\mathbf{F}$	=	force vector (subscripts r, $\theta$ , z denote cylindrical components)
FRC	=	field reversed configuration
$\phi$	=	magnetic flux
$\mathbf{I}$	=	current (subscripts r, $\theta$ , z denote cylindrical components)
$I_{sp}$	=	propellant specific impulse
$\mathbf{j}$	=	current density (subscripts r, $\theta$ , z denote cylindrical components)
$k$	=	Boltzmann's constant
$\eta$	=	plasma resistivity
$\eta_e$	=	thruster efficiency
$\lambda$	=	ratio of plasma radius to classical skin depth $\delta$
$\mu_0$	=	magnetic permeability in vacuum
$m$	=	electron mass
$\nu_{ei}$	=	electron-ion collision frequency
$n$	=	plasma density
$n_e$	=	electron density
$N$	=	electron line density
$p$	=	plasma pressure
$\theta$	=	azimuthal cylindrical coordinate
$Q$	=	circuit quality factor
$r$	=	radial cylindrical coordinate
$r_p$	=	plasma radius
$r_s$	=	magnetic separatrix radius

---

<sup>1</sup> AIAA Senior Member

<sup>2</sup> AIAA Member

<sup>3</sup> AIAA Member

RMF	= rotating magnetic field
T	= plasma temperature
$T_e$	= electron temperature
$\tau$	= RMF pulse length
$\omega$	= angular frequency of RMF
$\omega_{ce}$	= electron angular frequency in rotating field
$\omega_{ci}$	= ion angular frequency in rotating field
z	= axial cylindrical coordinate

## I. Introduction

The Electrodeless Lorentz Force (ELF) thruster creates a high-density, magnetized plasmoid known as a Field Reversed Configuration (FRC) employing a Rotating Magnetic Field (RMF). The RMF driven azimuthal currents, coupled with the enhanced axial magnetic field gradient produced by the FRC inside the flux preserving conical thruster, produce a large axial  $J_{\theta} \times B_r$  force that accelerates the plasmoid to high velocity. The ELF thruster has been demonstrated to successfully, and at high efficiency, ionize and electromagnetically accelerate xenon, nitrogen, and oxygen propellants. A schematic and photograph are shown in Figures 1 and 2.

This ability to utilize ambient gases enables a wide range of far-term applications. Nearest term, an air-breathing, solar electric orbital transfer vehicle operating in a highly-eccentric Geostationary Transfer Orbit is possible that requires virtually no onboard propellant. While adding to spacecraft complexity, it allows for the effective utilization of many tons of ambient propellant. While requiring advances in energy storage and utilization technologies, the final mission payoff is extreme. And finally, for interplanetary travel the ability to harness in-situ resources from non-terrestrial planetary atmospheres and water-containing asteroids allow sample and return and manned missions at a fraction of the propellant mass fraction of traditional missions.

Presented is a description of upgrades made to the 30 kW ELF thruster enabling operation on liquid water and complex carbon dioxide gaseous propellants.

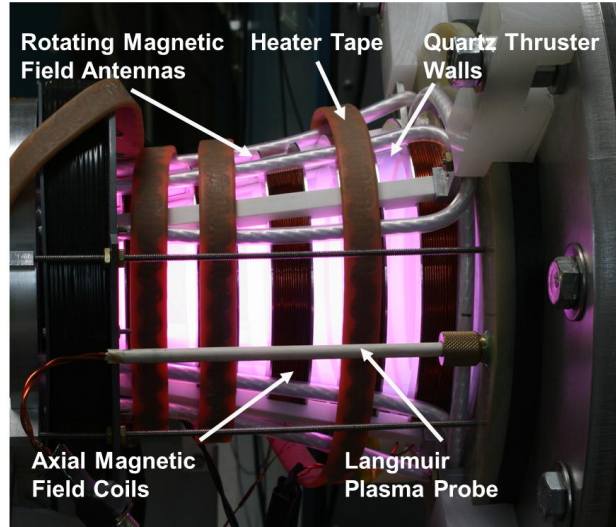
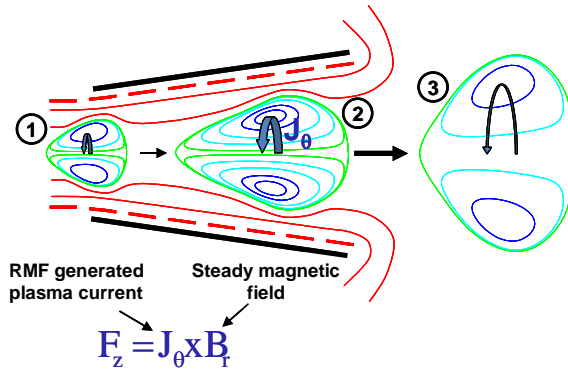


Figure 1. ELF thruster operating on water vapor.

## II. Background of the Electrodeless Lorentz Force Thruster

The ELF creates a high-density, magnetized plasmoid known as a Field Reversed Configuration (FRC) using external RF antennas that produce a Rotating Magnetic Field (RMF) throughout the thruster, transverse to the thruster axis of symmetry in the  $r-\theta$  plane. The synchronous motion of the electrons magnetized in this field produce a large azimuthal current, that when driven in a direction opposite to that flowing in the external solenoid, reduces and eventually reverses the magnetic field inside the plasma, thus forming a closed magnetic field configuration separate from the external thruster fields (the FRC). These large FRC plasma currents together with the greatly increased radial magnetic field created by the presence of the plasmoid result in a very substantial  $J_0 \times B_r$  force that rapidly accelerates the FRC propellant out of the thruster (Figure 2) [1, 2]. The axial force is thus overwhelmingly determined by the driven  $I_0$  and resultant  $B_r$  rather than thermal expansion forces. However, as in any expanding magnetic field, the expansion of the FRC with the thruster cross section as it is ejected provides for the conversion of the FRC thermal energy into directed energy minimizing the frozen flow losses and maximizing efficiency. This thruster has been detailed in several other papers [3] and will only be described in brief.

The technique of generating azimuthal electron currents in a plasma column by means of rotating magnetic fields was first investigated by Blevin & Thonemann in 1962 [4]. The principles of their technique can best be understood as follows. Consider that a transverse rotating magnetic field completely penetrates a cylindrical plasma column as in Figure 3. Provided that the angular frequency  $\omega$ , of the rotating field lies between the ion and electron cyclotron frequencies ( $\omega_{ci}$  and  $\omega_{ce}$ ) calculated with reference to the amplitude of the rotating field,  $B_\omega$ , and provided that the electron collision frequency is much less than the electron cyclotron frequency, the electrons can be considered as 'tied' to the lines of force of the rotating field. With the assumption that the electron collisions are relatively infrequent ( $\nu_e \ll \omega_{ce}$ ), they will circulate synchronously at the angular frequency  $\omega$ , whereas the ions (at least over the time of interest) have no net azimuthal motion. The electrons thus form a steady azimuthal current (in fact, the Hall current). In most systems, Hall currents are inhibited by electric polarization fields. In the situation under discussion, however, charge separation does not occur because of the azimuthal symmetry.



**Figure 2. ELF Thruster Operation: (1) Rotating Magnetic Fields (RMF) form high-density, FRC plasmoid (2) FRC grows and accelerates driven by RMF generated currents & steady field (3) FRC expands as ejected, converting any remaining thermal energy into directed energy.**

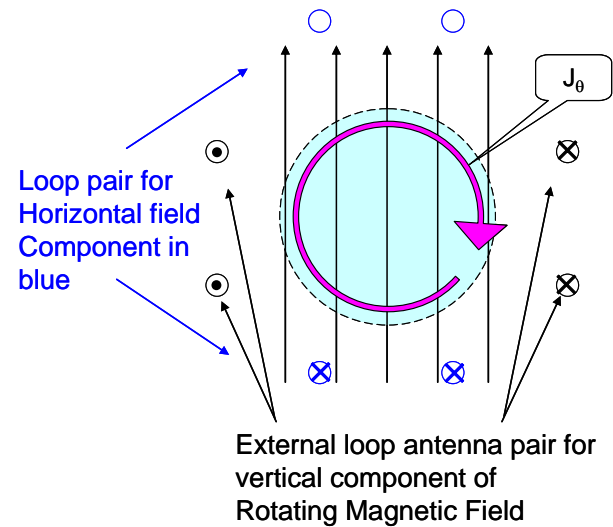


**Figure 3. Schematic of the cross section of the plasma column and RMF lines of force. The coil set of axial conductors employed to generate the RMF are also shown. These two orthogonal sets, carrying sinusoidal currents phased  $90^\circ$  apart, produce an  $m=1$  rotating magnetic field of constant amplitude.**

It should be noted that the frequency condition for current drive:

$$\omega_{ci} < \omega < \omega_{ce} \quad (1)$$

The antenna geometry for generating the RMF are not unique to this application. In fact, the same antenna configuration and RF frequency requirements (Eq. 1) are found for the propagation of the helicon wave as well [3, 4]. The singular difference between the helicon discharge and the full electron entrainment found with FRC generation is the magnitude of  $B_\omega$ . Both rely on the  $m=1$  transverse mode penetrating the plasma and coupling to the electrons. This is accomplished with the rotating field in the case of a two phase antenna. The right hand circularly rotating component of the oscillating field produced by a single  $m=1$  “saddle coil” antenna commonly employed for helicon discharges.

For the particular choice of field geometry and rotation frequency given in the above description, the appropriate form of Ohm's law is:

$$\mathbf{E} = \eta \mathbf{j} + \frac{1}{ne} (\mathbf{j} \times \mathbf{B}) \quad (2)$$

Steady-state solutions satisfying this equation can be obtained in two limits. In the limit of interest which leads to the formation of the FRC considers the  $\mathbf{j} \times \mathbf{B}$  term in Ohm's law to be dominant. The solution in this limit was originally obtained by Blevin & Thonemann [2], which describes the penetration of the rotating field into the plasma column and is described by Eq. 3. Additionally, it can be shown that the change in external magnetic field when the Hall term is completely dominant and the electrons are all in synchronous rotation is given by Eq. 4.

$$\mathbf{j}_\theta = -\frac{1}{\mu_0} \frac{\partial B_z}{\partial r} = -ne\omega r \quad (3)$$

$$\Delta B_z^M = B_z(r_p) - B_z(0) = \frac{\mu_0}{2\pi} e\omega N \quad (4)$$

This bulk rotation and increase in external magnetic field will result in a plasma configuration, the FRC, that is completely disconnected from external magnetic field coils and structure. At this point, the FRC is able to freely translate or be compressed by an applied field.

Thruster acceleration efficiency can easily be determined and described. The kinetic energy imparted by the magnetic expansion section can be given by the following analysis. Equation (5) describes the energy imparted on an FRC that is balanced by magnetic pressure between two states, a high-temperature, high magnetic field, and a low temperature, low magnetic field regime. Clearly, this approximation tends to break down at very low temperature, but during the expansion process it is typically found that an FRC will convert a majority of its thermal energy to kinetic energy when moving into a low field region. In the ELF thruster the plasmoid has a downstream residual electron temperature of 5-10 eV and total temperature of 10-20 eV as measured by magnetic field and double Langmuir probes.  $\eta_{th}$  is given as the conversion efficiency which is found to be 85-95 % with no additional flux conserving or expansion regions. This conversion efficiency could be readily increased with the addition of a low mass, passive magnetic expansion ring just outside the thruster exit. The magnetic pressure balance is given in Eq. (7).

$$E_K = \frac{5}{2} nk(T - T_0) \quad (5)$$

$$\eta_{th} = \frac{T - T_0}{T} \quad (6)$$

$$nkT = \frac{B_{ext}^2}{2\mu_0} \quad (7)$$

Finally, using the separatrix radius at the exit of the cone (in this case taken as the average radius) gives the total kinetic energy imparted on the FRC on its exit, for various conversion efficiencies,  $\eta_{th}$ .

$$E_{K\_Th} \approx \eta_{th} \left( \frac{B_{ext}^2}{2\mu_0} \pi r_s^2 l_{ac} \right) \quad (8)$$

FRC based propulsion utilizes high density plasma that is formed and ejected in  $\sim 20$   $\mu$ sec. Complete ionization happens in less than 1  $\mu$ s. This rapid, high-collision-rate ionization process is exceedingly efficient and minimizes wall collision, recombination, and radiation loss mechanisms. This is of interest because ionization is a major loss mechanism in traditional electric propulsion devices, and is particularly dominant at low specific impulses (particle kinetic energy) in electrostatic thrusters. This ionization loss energy is the full energy required to get a neutral particle to the exit of the thruster and includes radiation, excitation, recombination, electron bombardment ionization, and wall energy losses. A basic analysis of plasma ionization, excitation, and charge-exchange collisions for a given plasma temperature and density show that increasing density and/or temperature drastically decreases excitation and ionization losses [7]. Additionally, pulsed plasmas even further reduce radiation losses due to the time required for excitation. It has been demonstrated that ionization energies approaching the theoretical minima can be achieved in a pulsed inductive source of this type. For the temperature and densities of the ELF thruster the expected ionization potential and excitation energies are 20-40 eV/ion, dependent on propellant and operating condition. Finally, the magnetic confinement of an ELF thruster drastically reduces wall collisions. Therefore, given a per-ion ionization and excitation loss of 40 eV/ion, ionization losses are simply:

$$E_{ion} = \frac{m_{bit}}{M_0} * 40[eV] * e[J/eV] \quad (9)$$

$M_{bit}$  is the total propellant mass in the FRC and  $M_0$  is the atomic mass of the propellant. Ohmic coil losses are taken to be the resistive losses in the magnetic coils ( $R_{Coil}$ ), capacitors, transmission lines and antenna ( $R_{circuit}$ ) over the discharge length. Bias capacitor bank and pre-ionization circuit are simply the energy utilized in the bias and pre-ionization discharge circuits during the discharge.

$$E_{\Omega} = \Delta\tau(ESR + R_{Coil} + R_{Circuit})I_{RMS}^2 \quad (10)$$

$$\eta_{ELF} = \frac{E_{K\_RMF} + \eta_{th} E_{th}}{E_{K\_RMF} + E_{th} + E_{ion} + E_{\Omega}} \quad (11)$$

The thruster efficiency  $\eta_{ELF}$  can now be evaluated:

where  $E_{th}$  is the total thermal energy input into the FRC. Using representative numbers from a Xenon, 50 J ELF discharge, with a separatrix radius  $\sim 0.8r$  and measured density and mass bits the following table can be compiled. It can be clearly seen that for these operating conditions an RMF FRC system can be highly efficient as shown in Table 1.

Energy Terms for 50 J total input	Contribution
Kinetic - RMF Acceleration – $E_{K\_RMF}$	40
Kinetic – Thermal Expansion – $E_{K\_th}$	8
Thermal – Unrecovered $(1-\eta_{th}) E_{th}$	<1
Ionization, Excitation, and Wall Losses - $E_{ion}$	2
Ohmic – Antenna and Capacitor resistance	2
Ohmic – Bias coil and flux coil resistance	<1
Ohmic – discharge initiator (PI)	<1
<b>Total Thruster Efficiency</b> (from Eq.11)	<b>85+%</b>

Table 1. ELF Energy Distribution

It is important to note that the performance, and thus the analysis, of high-Beta thrusters are radically different from pulsed inductive thrusters. In traditional pulsed inductive thrusters [8], kinetic energy is added to the plasma simply through  $J \times B$  forces between the plasma current and the applied magnetic field. The plasma itself generates little magnetic field and has no stored inductive energy. Typically conical pulsed inductive thrusters balance circuit rise times, plasma lifetimes, and cone angles to maximize the effective axial force on the plasma during the stroke. In FRC thrusters, the plasma has significant stored inductive energy and plasma pressure. The driving circuit can continue to heat, add energy, and add inductive energy to the propellant plasma to much higher levels than a low energy current sheet thruster. The effective stroke then is the plasmas ejection from the thruster body itself. In this ejection process, pressure balance is maintained and plasma inductive and thermal energies are converted to directed, axial kinetic energy. This is analogous to thermal expansion in traditional chemical rockets, only the plasma boundary is the magnetic field rather than the thruster body. The limits to this process are no longer inductive or circuit losses, but rather the radial diffusion time of the plasma across the axial magnetic field and into the thruster body. Efficiency can then simply be determined by examining the change in plasma pressure between the compressed state and the downstream state.

### III. Hardware Description of the 30 kW ELF Thruster and Liquid Propellant Injector

#### A. 30 kW ELF Thruster

The 30 kW ELF thruster consists of a truncated conical quartz chamber/insulator 3 mm in thickness, 20 cm long, large radius of 10 cm, and a cone angle of 12 degrees. it is mounted to the outside of the MSNW large vacuum facility. The thruster is currently operated in air for diagnostic and timing purposes, with the plume projecting into the chamber. This quartz insulator has 6 aluminum flux conservers and bias field magnets. These magnets provide the initial and insulating magnetic field that insulates the thruster walls from the high pressure FRC as well as providing part of the accelerating field. RMF antennas are configured in the standard “Saddle”,  $m=1$  antenna configuration. The antennas are constructed from high-Q Litz wiring (4200 individual, parallel wires) that are insulated in high-temperature Tef-Zel insulation. The switch and capacitor assemblies located close to the thruster and fed with 2 inch wide stripline. Figure 4 shows a labeled cross section of the thruster, Figure 5 shows the ELF attached to the side of the vacuum facility

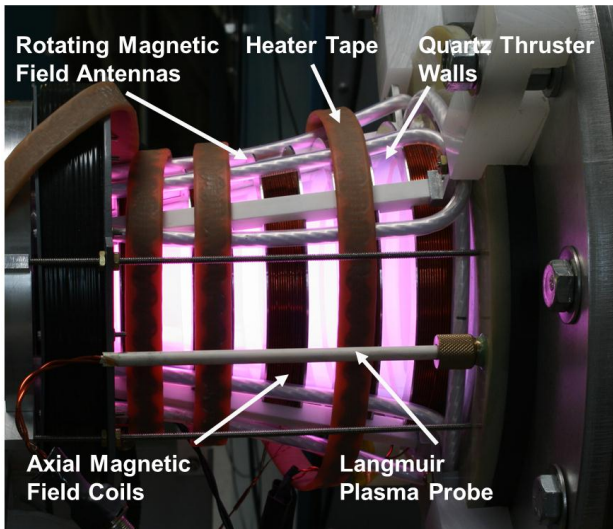


Figure 4. Cross Section of the ELF thruster with labeled components, operating on water vapor.

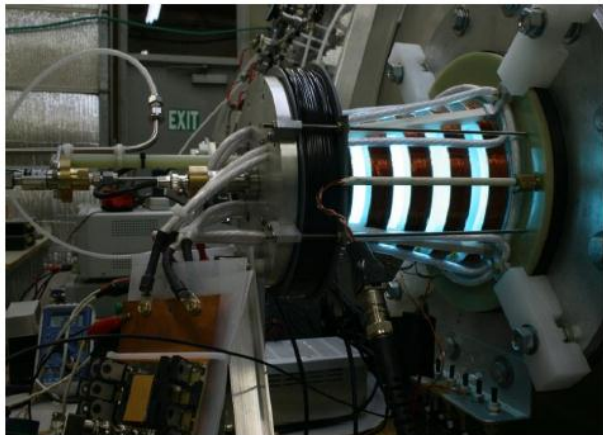
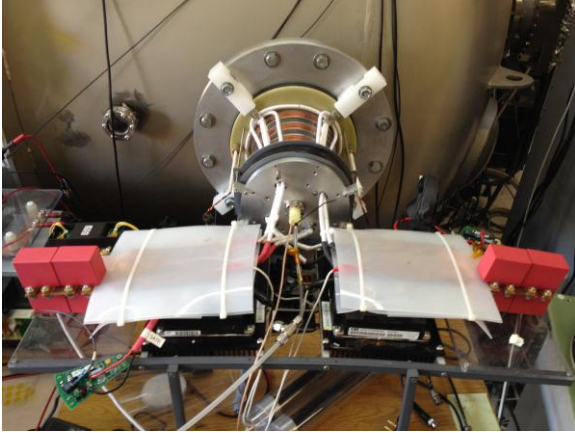
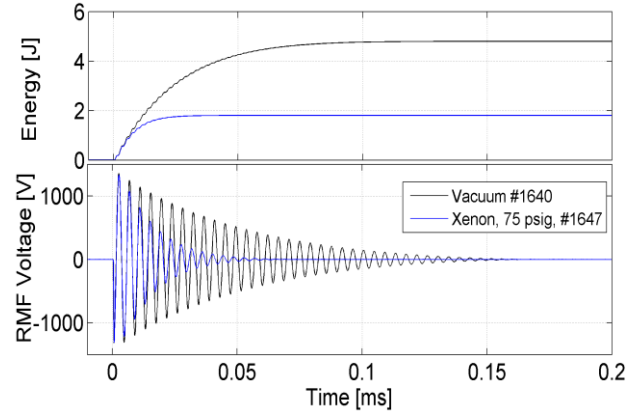


Figure 5. The 30 kW ELF thruster, trim coil, bias field coils, RMF antenna, and high-energy switches operating on Xenon.



**Figure 6. 30 kW ELF thruster experimental setup for operation on water and carbon dioxide propellants.** Shown are high-Q capacitors, high-power ABB IGBT switches, RMF antennas, and low inductance stripline feed.



**Figure 7. Time resolved plot of a typical Xenon FRC energy loading.** Shown is the integrated energy deposited in the discharge coil for both vacuum and plasma discharges. The instantaneous capacitor voltage is shown as energy is deposited in the plasma.

## B. PPU

The 30 kW ELF power processing unit (PPU) uses the standard MSNW RMF a pulse charging supply. This PPU was operated with a bus voltage of 300 volts that is then inductively and at high efficiency pulse charges the onboard capacitors to 2800 volts. This inductive pulse charging used a 4 microhenry air-core inductor with a 1.2 microfarad high-Q capacitor [9]. The repetition rate was varied by fiberoptically triggering the IGBT switches at various average rates. The peak charging voltage could be varied by changing on time, charging time, and bus voltage. For the data to be described in the following sections this thruster was operated with a repetition rate of 100 to 1500 Hz. The RMF discharge antenna is as described in other papers [1] and used high temperature, low resistance, Litz wire. The switches are high power ABB, IGBT switches that have local heat sink cooling. The charging time for the following data was 450 microseconds with a pulse charging peak current of 40 amps. Shown in Figure 6 is a picture of the entire experiment set up including both antenna phases, high efficiency capacitors and pulse charging inductors. The wave form for a vacuum and plasma discharge case is shown in Figure 7 and Figure 8. The operation was varied over a range of repetition rates by varying the time between discharges. The charging time was maintained constant and the resulting RMF discharge energy and voltage was maintained constant.

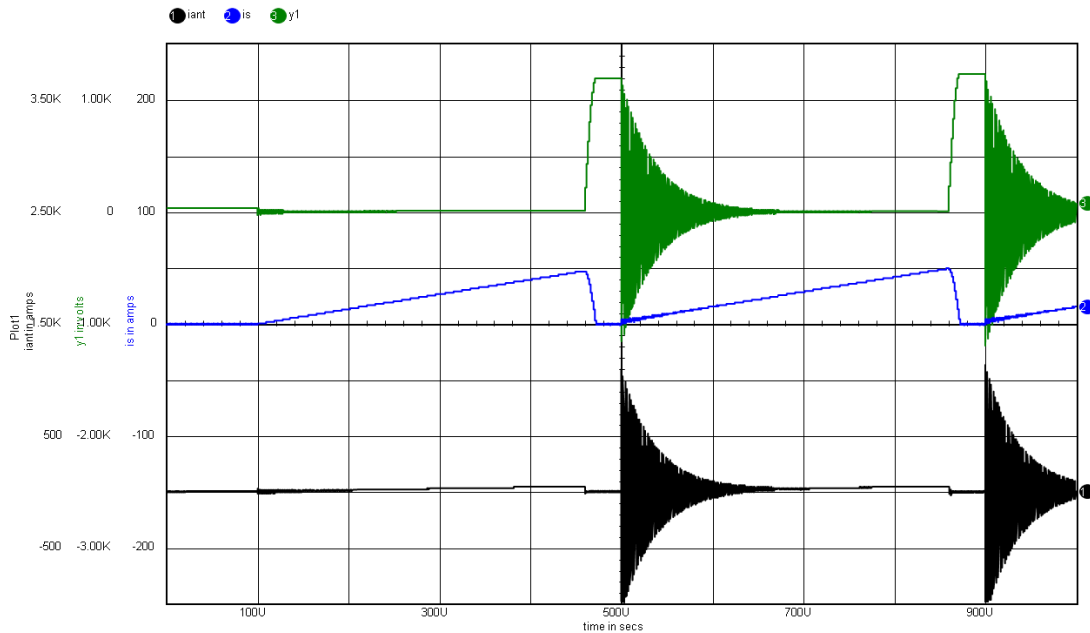


**Figure 8. Circuit results. Shown is a 2 kHz discharge frequency with a 300 kHz RF frequency. Shown in green is capacitor voltage, blue is battery draw, black is antenna current.**

The key component for this investigation of non-traditional propellants in the propellant injector. This injector was an integrated pre-ionization injector, with external heater, and porous tungsten propellant feed. The electrode geometry consists of a hollow 0.3 inch diameter tube with a 0.125 inch bore. This tube is unterminated and is a hollow cylinder. Schematics of the electrodes are shown in Figure 9. An inner tungsten electrode was press-fit into the cylinder to be used as a anode as well seal the porous tungsten bore. Finally, the anode was a machined molybdenum nozzle to both push the current sheet downstream and allow for proper warm gas expansion. This Molybdenum electrode was then isolated with an Alumina outer sheath which supported a nichrome heater coil, again potted with alumina. Several characteristics of this design are innovative and critical to this task. The thermal coefficient of expansion of Alumina, Molybdenum, and Tungsten are all quite similar thereby reducing any thermal stress or thermal expansion issues expected. Additionally, all these materials are compatible with water and are designed for long life. The entire assembly was heated to 10-200 C.

The 80% porous tungsten electrodes performed as expected. With a pure water propellant, the heated porous tungsten performed excellently, showing clear transition from frozen to pure vapor emission (25 C) into the vacuum chamber. Well over 1 kg was vaporized through this electrode.

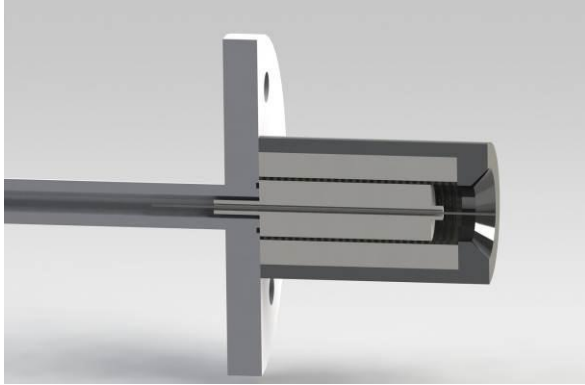


**Figure 9. Cross section schematic of injector.**

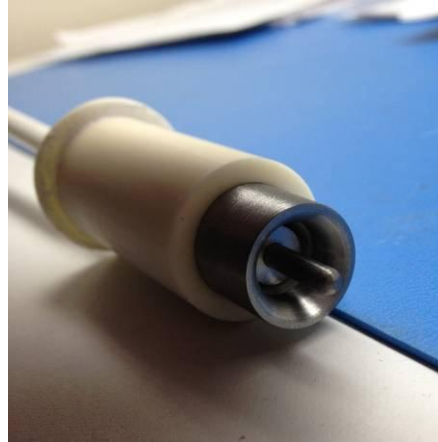


**Figure 10. Completed Molybdenum-porous tungsten PI.**

#### **D. Gaseous Propellant Feed**

Several major facilities upgrades have been implemented to support testing of the FRC thrusters at MSNW on a variety of propellants. First a new flow system has been implemented that can incorporate three gas mixtures as well as two gas flow ranges (0-50, 0-500 sccm) with a single thruster. This system uses a standard plenum-calibration architecture and uses Alicat mass flow controllers for dynamic propellant operation. The flow system is shown Figure 12. This flow system has demonstrated the ability to be operated in both a long-pulse mode as well as steady state. The required labview drivers and programming to allow for a 10 ms to 10 hr long gas flow have been implemented.

As part of thruster development efforts several large turbo-molecular pumps and a cryogenic-collar have been added to the MSNW BC vacuum facility. This 2 m by 3 m chamber has greater than 10,000 Liters of pumping on Xenon and due to the isolated cryo-collar can be pumped down to operating pressure in less than 8 hrs. Finally, by using turbo-molecular pumps this facility is fully compatible with lightweight gases and can pump them at high speeds. An internal photograph of the upgraded facility is shown in Figure 11.



**Figure 11. MSNW large vacuum facility.**

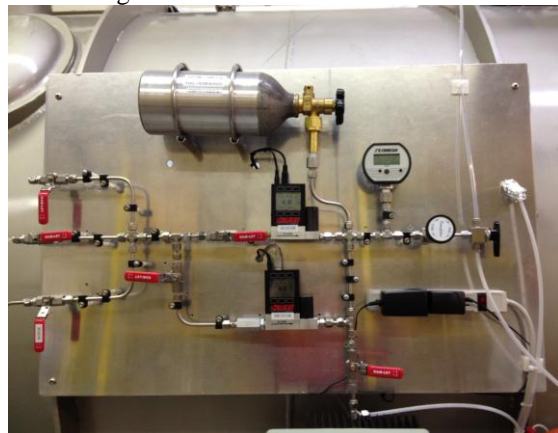


**Figure 12. Three gas flow system, flow controllers, and plenum calibration.**

## IV. Operational Description

### A. Chamber Operation

The large MSNW vacuum facility was used for these tests as describe above. No significant challenges were see during testing at MSNW on pure water vapor or carbon dioxide. The large, stainless facility and flow rates of 1-30 mg/s yielded no condensation or pumping problems. Ultimate base pressure usually was obtained required approximately 1 hour after water flow cessation. The chamber had a pressure of 7E-4 Torr at 8 mg/s and a base pressure of 5E-7 Torr.

### B. Water Injection

Water injection was accomplished by means of a peristaltic pump (Control Company Mini-Pump Variable Control) and external resistive heaters. As was described earlier, a porous tungsten electrode served as both the pre-ionization cathode, as well as the primary flow restriction for the liquid propellant. Flow rate was maintained by the flow velocity setting on the peristaltic pump, as well as an external flow meter. This liquid flow meter was simply calibrated with a known volume and the flow described in the following tests was set to 28 milliliters per hour (8 mg per second). The porous tungsten served as the primary flow restriction and it is believed that the flow system contained liquid water up to the tungsten. The input line and porous tungsten was maintained at 25 degrees Celsius and for this non-optimized set up required an input energy of approximately 50 watts to maintain liquid flow through the porous interface. As expected, with no external heat the porous interface quickly became clogged with water ice. The thermal couple was imbedded in the preionization insulator and is expected to have been highly representative of the temperature of the water and inner surface of the tungsten.

### C. Pre-Ionization

Thorough ionization was initiated with a standard MSNW triggering circuit. This particular triggering circuit had a peak voltage of 1 kilovolts was isolated through a high efficiency air core transformer from the driver's circuit. (inaudible) would be data collected. Any preionization of greater than 500 volts would be sufficient to breakdown water vapor. Finally, there was no evidence of water droplets, water condensation or liquid water in the thruster body or vacuum facility. The current waveform for the PI circuit is shown in Figure 13. In the following tests, it is important to note that for any number of FRC discharges only a single preionization was required; therefore, minimizing required operational duty cycle and energy is by the preionization system.

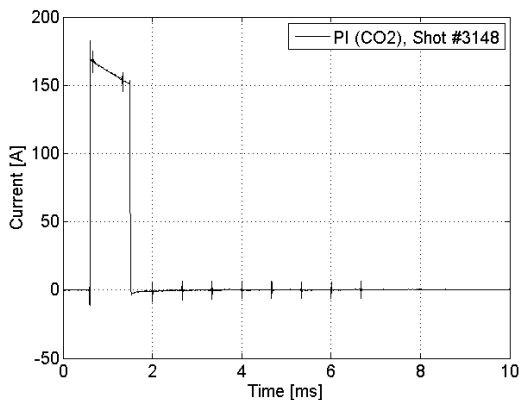


**Figure 13. PI Waveform for carbon dioxide. 1 kV charge voltage, Shot #3148.**

#### D. FRC Discharges

Figure 6 and 14 show a typical discharge. The curve in black (bottom) shows the antenna circulating energy (from capacitor voltage), oscillating at 300 kHz with no gas puff in the cone. It has a distinct rise as power is transferred to the antenna circuit (the secondary or load) from the capacitor and switching circuit (primary). The blue curve shows identical operating parameters, but with a gas and pre-ionization added. The initial power transfer to the circuit is identical in both cases, however, it can be clearly seen when the bulk ionization and current drive occurs ( $\sim 50 \mu\text{s}$ ). The circuit then loads and the current drive in the plasma is significantly increased. The change in current between a vacuum and plasma case shows the efficiency of coupling.

Axial magnetic field loops were arrayed externally along the discharge cone to measure the diamagnetic current drive in the cone. These measurements give an indication of the location of the separatrix and the amount of compression experienced by the FRC plasma. A compression ratio of 2 ( $B_{\text{ext}}/B_{\text{bias}}$ ) is typical of a well-formed RMF FRC. Figure 14 shows the typical response and formation of a Xenon FRC in the ELF. As the loading begins and current drive is initiated in the RMF antennas, a spike in diamagnetic current is measured at the base of the cone, typical on the order of 10-50%. This current drive continues to progress axially down the cone, building in strength (ratio) and forming a well-defined leading edge. This implies that an FRC is both being formed axially and accelerated axially. As can be seen in Figure 14 when the bulk current and plasma is at the exit of the cone there is little or no plasma at the small end of the cone.

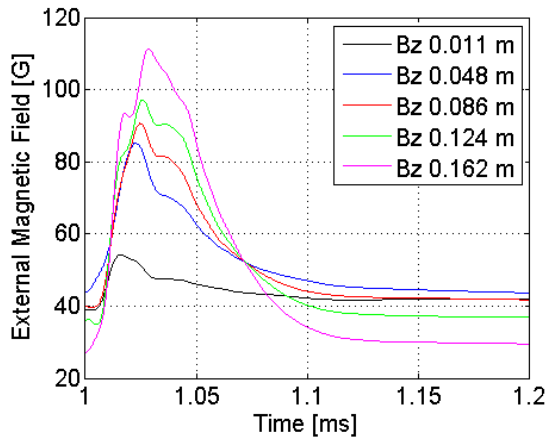


Figure 14. Slow bias field as well as the pulsed flux compression due to the formation and passage of the Xenon FRC discharge.

#### E. Downstream Diagnostics

A range of standard diagnostics is used to fully characterize a translating FRC. External magnetic field probes characterize the magnitude of diamagnetism and can directly yield the particle pressure of the FRC. These probes have been calibrated to 300 and 30 kHz operation and have an accuracy of  $6\text{E}-5$  turns/ $\text{m}^2$  at each of the 6 axial probe locations.

Internal double Langmuir probes resolve transient plasma density at less than 1 microsecond resolution are implemented in the standard “hook” formation [10]. These probes are asymmetric double Langmuir probes with an ion saturation collection area of  $50 \text{ mm}^2$  and are swept from  $-36$  to  $+36$  volts. They are fed from the outside of the chamber, shown in Figure 4. They are swing arm probes which have a positional cord that can be swept with along the entire width of the thruster. This results in a composite 30 cm axial and 15 cm radial range. And finally, external magnetic flux loops are used to characterize the total plasma trapped flux as well as flux leakage through the external flux conservers. These diagnostics are the traditional FRC thruster diagnostics and are well documented in [3] and [10].

#### F. Martian Atmosphere Simulant

In the propellant feed and mixing system shown in Figure 12, a simulated Martian atmosphere was composed. This was accomplished by filling a  $1692 \text{ mm}^2$  plenum with 95% high-purity, oil-free carbon dioxide, 3% UHP research-grade nitrogen, and 2% Argon. In this implementation the high-flow flow controller was used at 500 sccm to fill the plenum. Gas ratios were altered varying the fill time of each of the propellants. Then plenum was filled to 60 psi, or approximately 15 grams of propellant per charge. The system was then rerouted so that the plenum was used as the gas source and the 0-500 sccm flow controller was used to provide flow. It is expected that the nitrogen provided little change in average performance, compared with pure  $\text{CO}_2$ . However, the small argon component would have decreased the initial ionization energy required to begin breakdown, yielding a small, but important,

initial increase in the rate of ionization. Approximately 150 grams of CO<sub>2</sub> mixture were processed during these tests.

## V. Experimental Results

### A. Operational Frequency

One of the key scaling metrics of the ELF thruster is repetition rate. In previous ELF Thruster and EMPT programs the repetition rate was carefully empirically determined, based solely on thruster performance. As shown in Figure 15, the optimal repetition period is roughly equal to the time it takes a cold, neutral gas to transit the length of the thruster body, as described by the equivalent length ( $Cs/f$  equal to  $l$ ). Interestingly, lightweight and molecular propellants typically scale to slower optimal fill times, likely due to energy absorbed into vibrational modes and wall equilibration. Therefore, the ideal repetition rate for a decomposed water propellant can be estimated using the average molecular speed of decomposed products. However, because the final products of the vaporized propellant will be a product of both the partially ionized and vaporized components of a heavy molecular gas, the optimal repetition frequency will have to be determined empirically. Therefore, this thruster design has been updated to include a variable frequency pulse charging circuit that can dynamically vary the repetition rate and therefore the thruster power as required. This optimal discharge frequency was determined by optimizing the excluded magnetic field at the thruster midplane, which corresponds to both the maximum inductive energy in the plasma as well as maximum Isp. It is expected that scaling to maximize thrust-to-power, rather than Isp, will lead to lower optimal frequencies.

Gas	Mass [amu]	Sound Speed (Cs) [m/s]	Equivalent Length ( $l/l_0$ ) [-]	Repetition Frequency (f)[Hz]
Xenon	131	169	0.85	1988
Argon	40	319	1	3190
CO <sub>2</sub>	44	267	1.1	2427
H <sub>2</sub> O*	18	405	1.1	3682

Figure 15. The measured scaling of ideal thruster repetition rate as a function of geometry and sound speed.

\*Calculated.

## B. Downstream Results in Martian Air

Operation of the ELF thruster on simulated Martian Air was quite successful. Martian Air was tested from 100-500 sccm into the MSNW large vacuum facility. Using the same techniques employed above and typically used in the 30 kW Xenon ELF thruster, the largely  $\text{CO}_2$  propellant was injected into the thruster and a pre-ionization discharge was initiated. The thruster was then pulsed charged with a 300 V bus voltage to 2700 V. The RMF oscillated at 220 kHz with this particular inductor and capacitor geometry. It was expected that the higher ionization energy, dissociation energy, and rapid recombination rate of  $\text{CO}_2$  would highly detrimentally affect the operation of the thruster. There was clearly some decrease in performance as will be discussed shortly, however, overall  $\text{CO}_2$  (the Martian Air mixture) was operated successfully with FRCs being formed and ejected from 500 to 4000 s Isp.

Figure 16 shows a long exposure photograph of Martian Atmosphere. This discharge is similar in color previous oxygen discharges, with a bluish-white emission. Figure 17 shows the results for downstream double Langmuir probes used for Time-of-Flight analysis. Three velocities are measured for each discharge by comparing several key characteristics of plasma density traces recorded. The leading edge gives an indication of the high velocity and initial rise of the plasma. The peak plasma data shows the location of the FRC null and maximum FRC momentum. Finally, the average moment of the plasma gives the velocity of the average ion in the FRC. This value is used as the average FRC velocity. Also, in a well formed FRC with well-positioned TOF probes, these three values will be similar. Shown in Figure 18 are nine translating FRCs that were formed and ejected at 1500 Hz and 20 km/s. Figure 19 shows the formation and ejection of one of the FRCs. This measurement uses the calibrated external magnetic field probes to measure the external magnetic field during formation and ejection. This clearly shows the initial, steady bias magnetic field, the initial ionization, field compression as the FRC expands and pushes on the flux conserver and magnetic geometry, and finally ejection. Figure 20 shows the steady operation of the ELF thruster. The high-speed Lanmguir probes are digitized and shown for 1500 Hz. In this case, the trace shows the peak Langmuir probe density value as the steady thruster operation evolves due to gas flow heating. The complex nature of the interaction of a steady operating, pulsed thruster is currently being investigated.

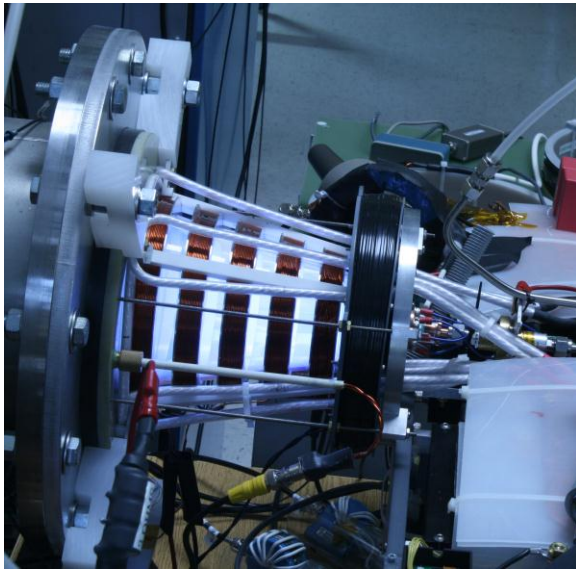


**Figure 16. Photograph of 500  $\text{CO}_2$  discharges.** Shown is 1500 Hz and 5.4 kW operation.

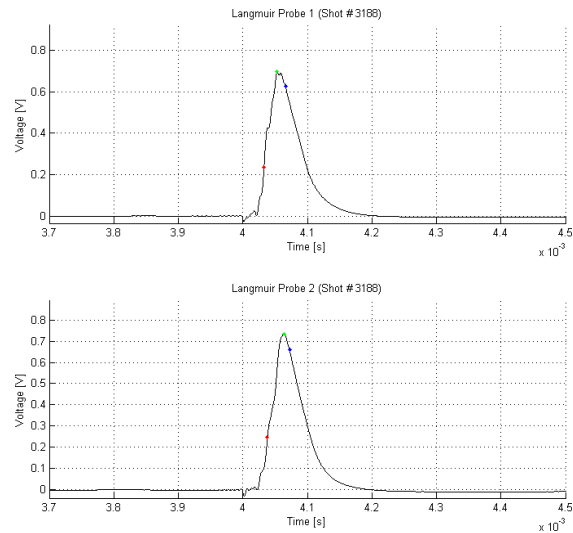


**Figure 17. Time-of-Flight analysis for  $\text{CO}_2$ .** Shown are the three velocity indicators, leading edge (red), peak (green), and central moment (blue) densities for two downstream double Langmuir probes.

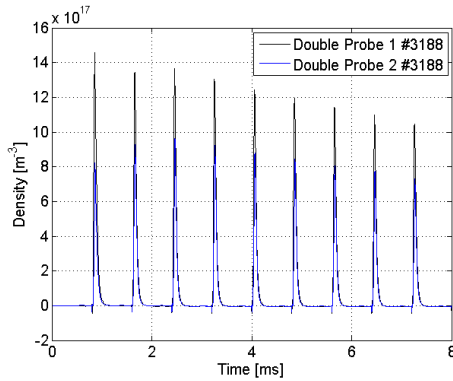


**Figure 18. Downstream train of simulated Martian Air FRC discharges. Shot #3188.**

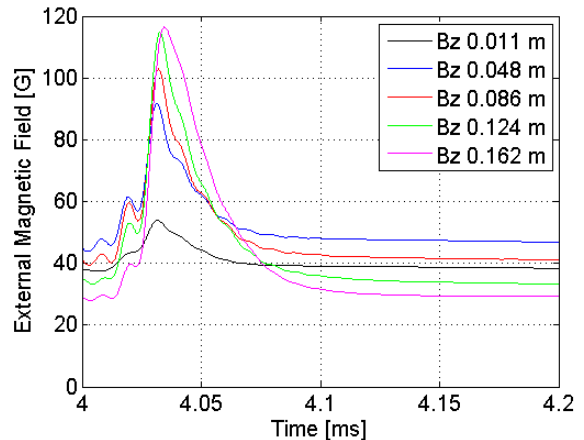


**Figure 19. External magnetic field, showing a well-reversed FRC formation and translation.**

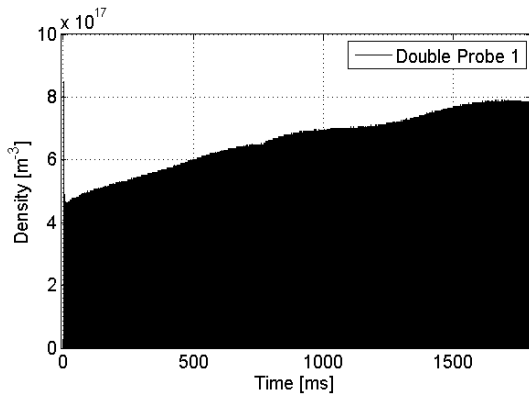


**Figure 20. Steady operation of the ELF thruster.**  
Shown is downstream Langmuir probe density for steady 1500 Hz operation.

Thruster operation at 1500 Hz and 250 sccm of Martian Atmosphere resulted in average FRC velocities of 19 km/s at 4800 Watts of thruster power. Increasing the flow to 500 sccm and the power to 5400 Watts of input energy into the thruster lead to FRC velocities of 17 km/s. These velocities are repeatable and calibrated to within 1 km/s. Steady operation of the thruster has been shown with a CO<sub>2</sub> and simulated Martian Air propellant. Additionally, it is clear that sufficient plasma velocities for high efficiency operation have been obtained. It is important to note, however, that while plasma velocities are required for high Isp, gas utilization is particularly key to proving steady, high Isp operation. Therefore, current work focuses on testing at higher repetition rates (2500-3000 Hz) as well as implementing thrust stand testing for 15-30 kW operation. Thruster repetition rates were limited for these test due to chamber and electrical limitations.

### C. Downstream Results in Water

Preliminary testing has been done with liquid water. As described above, the liquid water was fed into the thruster with a heated, porous tungsten electrode. This water flow was controlled with a liquid peristaltic pump and for the testing described below was a constant 8 mg/s (540 sccm of 'room temperature' water vapor).

Figure 21 shows a long exposure photograph of the ELF thruster operating on water vapor. This discharge is clearly dominated by Hydrogen emission lines and the thruster operation is similar to previously reported Deuterium discharges [11]. Figure 22 shows Langmuir TOF analysis for 540 sccm, similar to described above. However, in this case, TOF analysis is inconclusive. For the probe spacing in these tests, the leading edge velocities were greater than 50 km/s, while the bulk velocities were 17 km/s. This large discrepancy is due to two factors, the closeness of the probes and the separation of the Hydrogen and Oxygen plasma components downstream. The leading probe, 0.3 m downstream must be moved closer to the thruster while the downstream probe location is maintained. Further testing will demonstrate more accurate plasma velocities, though it is clear that the FRC has attained very high speeds, again suitable for Electric Propulsion application. Figure 23 shows 26 translating FRCs that were formed and ejected at 1500 Hz as they pass through the downstream probes. Velocity measurements have too great an error for suitable for further analysis. Figure 24 shows the formation and ejection of one of the FRCs. This clearly shows the initial, steady bias magnetic field, the initial ionization, field compression as the FRC expands and pushes on the flux conserver and magnetic geometry, and finally ejection. It is important to note that compared to a similar energy CO<sub>2</sub> or Xenon energy, the water-based plasma is significantly lower in pressure, temperature, and internal energy.

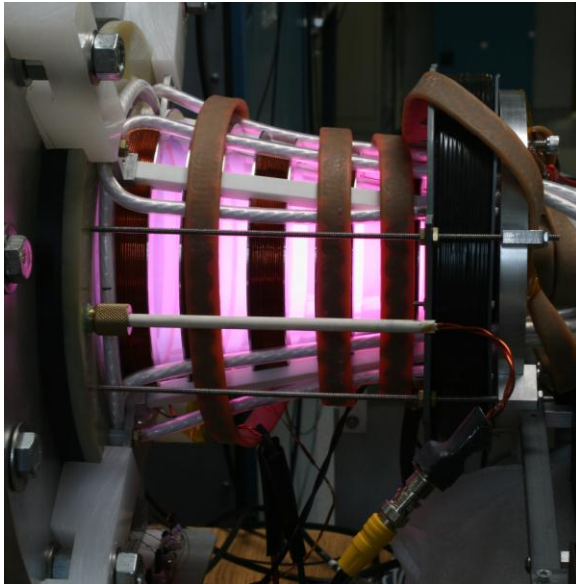


**Figure 21. Photograph of 500 H<sub>2</sub>O discharges.**  
*Shown is 1500 Hz and 2.0 kW operation at 540 sccm.*

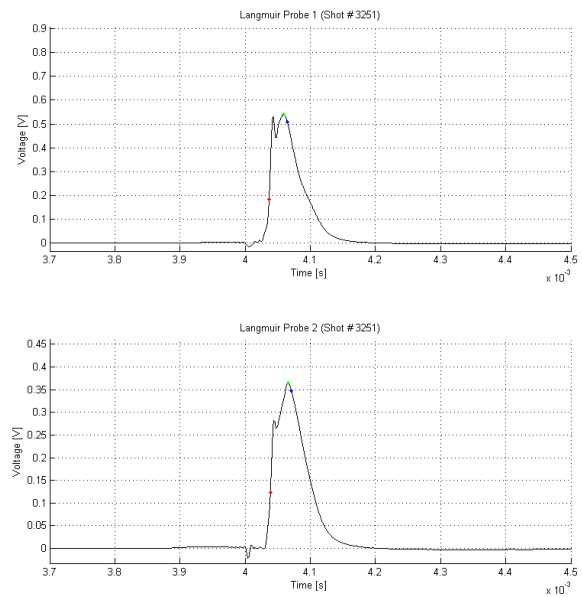


**Figure 22. Time-of-Flight analysis for H<sub>2</sub>O.** *Shown are the three velocity indicators, leading edge (red), peak (green), and central moment (blue) for two double Langmuir probes.*

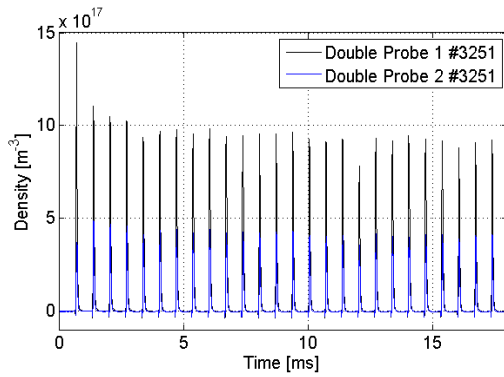


**Figure 23. Downstream train of H<sub>2</sub>O FRC discharges. Shot #3251.**

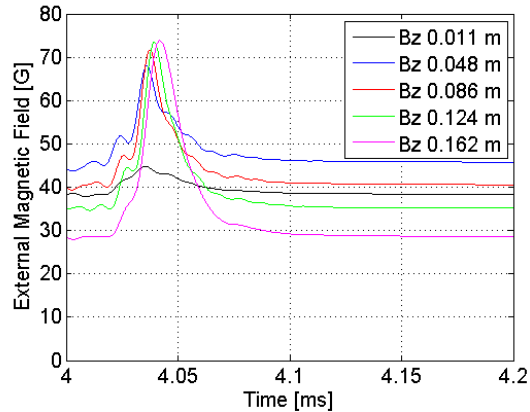


**Figure 24. External magnetic field, showing a well-reversed FRC formation and translation.**

#### D. Discussion and Future Work

In the presented work a concise discussion of FRC formation physics has been given. Additionally, a review of FRC acceleration mechanisms and overall expected thruster efficiencies are given for Xenon. The Electrodeless Lorentz Force thruster has now demonstrated the ability to ionize, compress, and electromagnetically accelerate simulated Martian Atmosphere as well as vaporized liquid water to velocities of greater than 15 km/s. The newly developed flow systems, liquid water injector, and thruster systems have been described.

Several interesting discoveries have been made in these experiments. As expected both Carbon dioxide, Martian Air, and water vapor performed worse than pure Xenon. They required more input energy and formed weaker, lower pressure, and slower-moving FRCs. This is not unexpected given their increased dissociation and ionization energies. However, this did not manifest itself in lower thruster efficiency, but rather lower coupling. As shown above, high specific impulses and high thruster efficiencies were attained, particularly considering the low average molecular weight of the propellant. Coupling of the PPU energy into the plasma, as shown above as ‘loading’ was decreased from a Xenon plasma with the testing described in this paper yielding 20-50% PPU efficiencies. Compare this with the 85+% Xenon PPU efficiencies that have previously been reported for the ELF thruster [3]. It is believed that this is primarily due to improper matching between the theoretical optimal repetition rates and the repetition rates actually tested due to chamber and electronics limitations. Future work will seek to expanding the operational regime and test higher average power, repetition rates, and peak energies. Perhaps most interestingly, the expected major challenges of propellant injection were not observed. In the steady operation of liquid water, using an adequate porous tungsten injector and low power heater was sufficient to maintain steady, well-behaved water vapor flow into the thruster. Martian atmosphere injection, pre-ionization, and FRC formation was demonstrated with steady flow gas and zero coking, deposition, erosion, or clogging issues.

#### Acknowledgements

The authors would like to thank AFRL for support of the Electrodeless Lorentz Force thruster program. Without their support of 30 kW Xenon thruster hardware and development, this effort could not have occurred.

## References

- [1] M. Tuszewski, "Field Reversed Configurations", Nuclear Fusion Vol. 28, 2033 (1988)
- [2] I.R. Jones, "A review of rotating magnetic current drive ...", Phys. of Plasmas, **6**, 1950 (1999)
- [3] Slough, J., Kirtley, D. E., Weber, T., "Pulsed Plasmoid Propulsion: The ELF Thruster," IEPC-2009-265, 2009
- [4] H.A. Blevin and P.C. Thonemann, "Plasma Confinement using an Alternating Magnetic Field", Nucl. Fus. Suppl. **Part I**, 55 (1962).
- [5] W.N. Hugrass and R.C. Grimm, "A numerical study of the generation of an azimuthal current in a plasma cylinder using a transverse rotating magnetic field", J. Plasma Physics, **26** 455 (1981).
- [6] Christine Charles and Rod Boswell, "Current-free double-layer formation in a high-density helicon discharge", Appl. Phys. Lett., **82**, 1356 (2003).
- [7] Lieberman, M. and A. Lichtenberg. *Principles of plasma discharges and materials processing*, Wiley, 2005.
- [8] Daily, C.L. and Lovberg, R.H. "The PIT MkV Pulsed Inductive Thruster". NASA Contractor Report 19115.
- [9] Kirtley, D., Slough, J., Pfaff, M., Pihl, C. "Steady Operation of an Electromagnetic Plasmoid Thruster". Joint Army Navy NASA AirForce Conference, 2011.
- [10] T. E. Weber, J. T. Slough, and D. Kirtley, "The ELF thruster experimental facility". Review of Scientific Instruments, 2012.
- [11] Slough, J., Kirtley, D., Weber, T. "Preliminary Performance Measurements of the Air-Breathing ELF Thruster". Joint Army Navy NASA Air Force Conference, Orlando Florida, 2008.